



Installed F404 Engine Noise Source Characteristics from Far-field Directivity Measurements

Matthew A. Christian¹, Kent L. Gee², Jacob B. Streeter³, Logan T. Mathews⁴
Brigham Young University, Provo, Utah, 84602

Alan Wall⁵
Air Force Research Laboratory, Wright-Patterson AFB, Ohio, 45433

Jon Paul Johnson⁶
Brigham Young University – Idaho, Rexburg, ID, 83460

Steven C. Campbell⁷
Ball Aerospace Incorporated, Dayton, OH, 45433

This paper presents an analysis of acoustic radiation characteristics of a T-7A-installed F404 engine, as derived from far-field measurements. Radiated directivity at different engine conditions is compared with contemporary investigations into Mach wave radiation. The peak directivity angles observed in the far-field are used to evaluate appropriate values for the convective Mach number. It is shown that velocity from the convective Mach number is approximately 70% of the centerline jet velocity, agreeing with contemporary supersonic jet noise literature. Spatiospectral maps from far-field data indicate the presence of spatiospectral lobes, like those observed in the near field. These spatiospectral maps also illustrate interference nulls caused by ground reflection interference. A ground reflection model is used to attempt to correct these errors. Using these corrected data, the overall sound power level is calculated and is used to find the acoustic radiation efficiency, a value rarely calculated for jet engines. The F404 OAPWL is proportional to U_e^8 subsonically, and U_e^3 supersonically. The efficiency at afterburner exists between 0.5% and 0.8%, exhibiting similar acoustic efficiency trends as those seen in launch vehicles 50 years ago.

I. Nomenclature

AB	=	Afterburner
BSN	=	Broadband shock-associated noise
c_a	=	Ambient speed of sound
c_j	=	Speed of sound in fully expanded jet

¹ Graduate Student, Department of Mechanical Engineering, AIAA student member
² Professor of Physics, Department of Physics and Astronomy, AIAA senior member
³ Undergraduate Student, Department of Physics and Astronomy
⁴ Graduate Student, Department of Physics and Astronomy, AIAA student member
⁵ Air Force Research Laboratory, Wright-Patterson AFB, Ohio, 45433
⁶ Professor of Physics, Department of Physics, BYU-Idaho
⁷ Ball Aerospace Incorporated, Dayton, Ohio 45433, USA

DI	=	Directivity index
FSN	=	Fine-scale structure noise
F_t	=	Thrust
\bar{I}	=	Time-averaged acoustic intensity
LSN	=	Large-scale structure noise
MARP	=	Microphone array reference point
M_c	=	Convective Mach number
MIL	=	Full military power (100% thrust)
MWR	=	Mach wave radiation
n_{out}	=	Outward-facing normal vector
OAPWL	=	Overall sound power level
OASPL	=	Overall sound pressure level
p	=	Acoustic pressure
S	=	Surface area
SPL	=	Sound pressure level
U_j	=	Fully expanded jet velocity
θ_{pk}	=	Peak radiation angle
\bar{P}	=	Time-averaged power
η_{ac}	=	Acoustic radiation efficiency

II. Introduction

Noise generated by high-performance afterburning military aircraft creates a risk of hearing loss for ground crew and is potentially disruptive to neighboring communities. To mitigate these possible concerns, jet noise reduction has been a subject of great interest. Casalino et al. [1], Greska et al. [2], and Seiner et al. [3] have, among others, shown different methods of reducing jet noise which have been tested and implemented with varying success. A thorough understanding of the noise characteristics of modern aircraft is critical to the development of these and future noise reduction efforts. As the knowledge of jet noise sources improves, so will the ability to model and predict jet noise.

Jet noise models should connect jet or engine parameters to the acoustic radiation. Two examples are the jet convective Mach number, which describes the Mach wave radiation angle (and potentially the far-field peak directivity) for supersonic jets, and the acoustic radiation efficiency (η_{ac}), which links the jet stream mechanical power to radiated acoustic power. This paper uses both observed directivity values as well as measured sound power levels and η_{ac} values to connect far-field acoustical measurements to a military-style engine's jet characteristics. The data used are from a GE F404-103 turbofan engine installed in the new Boeing/SAAB T-7A "Red Hawk," at engine powers from 50% thrust to afterburner (AB).

The seminal jet noise study by Lighthill [4] identified the nature of turbulent mixing and acoustic radiation. Even before Ffowcs Williams's theoretical description of supersonic jet noise radiation [5], experimental investigations were identifying changes in radiation for the subsonic and supersonic regimes. For supersonic jets, turbulent mixing-related noise has been identified more specifically as noise from both fine and large-scale turbulent structures (FSN and LSN), broadband shock-associated noise (BSN), and Mach wave radiation (MWR). Although Mach waves have sometimes been simply seen as efficiently radiating large-scale noise with no real distinction made (e.g., Tam and Hu [6]), Liu et al. [7] described them as different both in terms of frequencies and radiation angle. As seen in Vaughn et al. [8] MWR becomes a dominant noise source for supersonic exhaust from a tactical jet engine. Liu et al., Vaughn et al., and Leete et al. [9] observed MWR dominate at approximately 115° , with LSN being the primary noise source farther aft.

A complicating factor in understanding far-field jet noise radiation characteristics, and their link to source parameters, is multipath interference. Because far-field measurements are often made with elevated microphones – to avoid microclimate and roughness effects at the ground that can distort spectra and to realistically obtain levels and spectra at maintainer positions – ground-reflection gains and nulls are present in the measured spectra. This interference pattern superposed on the radiated spectrum complicates data interpretation and modeling. (Local meteorological variability can also cause multipath interference effects at frequencies of importance to full-scale jet

noise, but that is mostly beyond the scope of the present paper.) Accounting for ground reflections from an extended, large-volume source with coherence properties that vary with frequency is quite complicated, but some progress has been made in this area. Building upon the work of Daigle [10] and Johnson [11], Gee et al. [12] developed a model for finite-impedance ground reflections from extended coherent and incoherent sources through a turbulent atmosphere and applied it to spectra from horizontal, static rocket firings. The model's use in this paper represents the first application of the model elsewhere and should be treated as preliminary. Nonetheless, the corrections to the measured spectra more realistically remove the effect of ground reflections on overall level, sound power, and η_{ac} .

Historically, concepts of sound power and η_{ac} have been commonplace in acoustic analyses of rockets. These have proven to be useful, as they provide at-a-glance values that illustrate the overall acoustic performance of an engine as a function of its mechanical power output. Despite considerable scatter in the available data, Eldred [13] determined the η_{ac} of rockets to be approximately 0.5%. This topic has been recently discussed in a review article on launch vehicle noise by Lubert et al. [14]. For comparison, Mathews et al. [15] calculated η_{ac} for the Falcon 9 launch vehicle to be ~ 0.31 (but with no correction for ground effects). Although discussed by Franken [16] in his 1958 review of aircraft jet engine noise, sound power and η_{ac} calculations of military aircraft have been largely absent from jet noise literature. In this paper, the T-7A far-field directivity data, with corrections for ground reflections, are integrated [17] to obtain radiated sound power as a function of engine power. A major conclusion of this paper is that the results suggest that variation of thrust from an intermediate to afterburner condition for the installed F404 engine represents a transition from the subsonic to supersonic jet regimes. The overall sound power level (OAPWL) is shown to approximately transition from a proportionality of jet velocity raised to the eighth power (U_e^8) for subsonic cases (see Lighthill [4]) to $\sim U_e^3$ for supersonic cases, agreeing with the transition described experimentally by Chobotov and Powell [18] and theoretically by Ffowcs Williams [5].

This paper is organized as follows. After a discussion of data collection, overall and frequency-dependent polar directivity patterns are shown and tied to convective Mach number and interpretations of MWR and LSN. Next, the overall sound pressure level (OASPL) pattern is adjusted to remove ground interference effects, before calculation and discussion of the OAPWL, η_{ac} , and the overall radiation directivity index (DI).

III. Data Collection

Pressure waveform data were collected on the morning of August 18th, 2019, at Holloman Air Force Base, New Mexico. The T-7A "Red Hawk" is a new trainer aircraft developed by Boeing/SAAB and is equipped with a single General Electric F404-103 afterburn-capable turbofan engine. The aircraft was tied down to a run-up pad with the front of the aircraft facing the blast deflector to preserve the full jet plume. The aircraft was run at engine powers from idle to full afterburner, running at each engine power for 30 seconds. This cycle was repeated six times. This paper focuses on 82% N2 (50% thrust), 88% N2 (75% thrust), full military power (MIL), and afterburner (AB). Initial analyses into the far-field measurements showed significant discrepancies between the first two and last four runs. These differences, which significantly shifted the frequencies of interference nulls, are currently attributed to likely temperature gradient shifts around sunrise but are still being investigated. Rather than attempt to account for these differences, this paper only reports the average measurements of those last four runs. Further studies into the cause(s) of the differences will be pursued in the future.



Figure 1: T-7A “Red Hawk” tied down at Holloman Air Force Base (above). View from the aircraft looking out toward far-field microphones (below).

As described in Leete et al. [19], the origin of the coordinate system used in all analyses was set on the ground directly below the nozzle exit. The positive x -direction was defined as downstream from the nozzle, with the positive y -direction to the side of the data collection. The angles of the microphones in the various arrays are defined from the microphone array reference point (MARP), located 4.0 m (13 ft) downstream of the nozzle. While over 200 microphones were used for data acquisition, this paper focuses solely on the microphones along a 38 m (125 ft) arc and a 76 m (250 ft) arc. The 38 m arc is made up of 14 1/4" GRAS 40BD-NAH microphones, arranged from 30° to 160° at 10° increments. The 76 m arc consisted of 22 1/4" GRAS 46BD microphones were arranged from 30° to 160° , with a microphone at every 10° increment, with additional microphones in the at 5° increments from 30° to 60° , and again from 110° to 160° . For both arcs, each microphone was mounted 1.5 m (5 ft) off the ground. Due to hardware failure, data from the microphone at 130° in the 76 m arc were corrupted at AB and will not be used here. The microphones were connected to a National Instruments PXIe-1062 chassis with 4496 cards as well as an NI 8840 Quad-Core Controller. For the four runups described here, the data were synchronously sampled at 96 kHz. Further information regarding the data acquisition process is found in Leete et al. [19].

To provide values for the convective Mach number or mechanical power, jet parameters are required. As an estimate of the F404-103 parameters, Seiner et al. [3] and Ennix et al. [20] provide conditions for the F404-400 engine. Seiner et al. listed both the fully expanded jet Mach number and stagnation temperature as functions of the engine power. From these parameters, isentropic flow assumptions allow fully expanded conditions to be calculated. Ennix et al. listed both the fully expanded jet velocity and Mach number.

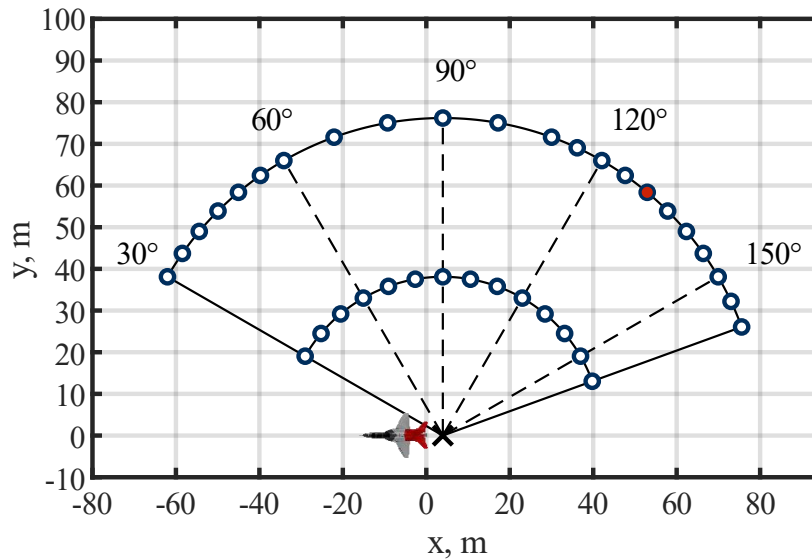


Fig. 2: Schematic of the microphone array along the 38 m and 76 m arcs. Microphone at 130° in 76 m arc shown in red to indicate the data corruption at that location.

IV. Analysis

A. Overall and frequency-dependent directivity

Overall directivity curves are obtained from the far-field data at each of the engine powers considered are shown in Fig. 3. The maximum OASPL, peak radiation angle, and radiation lobe width at each engine power are given in Table 1. Values for peak radiation angle and radiation lobe width were found using MATLAB's `pchip` interpolation function to estimate values between microphones at both far-field arcs. Radiation lobe width is defined here as the 3 dB-down lobe width (full-width, half-max). The radiation lobe width increases from intermediate thrust conditions to MIL and then remains approximately constant for AB. The reason for the MIL and AB lobe width being $\sim 5^\circ$ greater at the 38 m arc is not understood but may be caused by extended source effects such that the microphones are not truly in the far-field.

Table 1: Calculated values for maximum OASPL, peak radiation angle, and 3 dB down lobe width as functions of engine power.

38 m Arc				
Engine Power	50% Thrust	75% Thrust	MIL	AB
OASPL _{MAX} (dB)	115.3	127.1	134.1	138.3
Peak Radiation Angle	150°	150°	130°	120°
Radiation Lobe Width	27°	33°	38°	38°
76 m Arc				
Engine Power	50% Thrust	75% Thrust	MIL	AB
OASPL _{MAX} (dB)	109.6	121.7	128.7	132.5
Peak Radiation Angle	150°	140°	135°	120°
Radiation Lobe Width	23°	31°	35°	34°

In Fig. 3, the OASPL trends at both arcs reveal different trends at different angular ranges. Between 30° and 100°, there is a nearly uniform increase in OASPL with increasing engine power. Behind the aircraft, note a distinct, new lobe at about 110°-115° that appears at MIL and becomes more apparent at AB. Liu et al. [7] and Leete et al. [21] both recently published insights into the mechanisms of jet noise as observed from a large eddy-simulation (LES) of a heated, supersonic jet with conditions like that of afterburner. It was shown that noise from MWR was distinct from

noise generated from large-scale structures, with MWR noise dominating at approximately 115°. Though the peak radiation angle is at 130° for MIL, a distinct lobe is beginning to form between 115° and 125°. This lobe is even more evident at AB, where the peak radiation angle is 120°. These observations, as well as the lack of MWR lobes below MIL, indicate that the jet becomes supersonic at or just below MIL. This is reinforced by the near-field spatio-spectral maps shown by Leete et al. [19] and Olaveson et al. [22], where broadband shock-associated noise is present at both MIL and AB.

Historically, MWR is described as originating from supersonic, coherent, turbulent structures in the mixing layer of a jet, as explained by Tam and Hu [6] and Seiner [23]. The velocities of these structures, relative to the speed of sound of the fluid into which they radiate, are defined as the convective Mach number. The convective Mach number has been a subject of interest in the jet noise community to connect the peak radiation angle to jet parameters:

$$\theta_{pk} = \cos^{-1}\left(\frac{1}{M_c}\right). \quad (1)$$

With the peak radiation angle known, working backward from Eq. 1 provides an expected convective Mach number of the supersonically convecting structures. This expected convective Mach number can then be empirically related to the fully expanded jet velocity and ambient sound speed as

$$M_c = \frac{\kappa U_j}{c_a}, \quad (2)$$

where κ is an empirical parameter. For heated, supersonic jets Tam and Parrish [24] and Murray and Lyons [25] show a kappa value of between 0.6 and 0.8 seems to be the most appropriate. At MIL, the peak radiation angle measured from the 76 m arc is 130°. Equation 1 shows a convective Mach number of 1.41 would produce this peak radiation angle. Data from Ennix [20] and Seiner [3] were used to provide an estimation for U_j at MIL, which yields a value of κ between 0.64 and 0.7. Because the datasets from Ennix and Seiner did not include values at AB, it was assumed that the velocity increased by 50% from MIL to AB. A 50% increase in velocity is the same increase seen in the LES simulation reported by Chen et al. [26] when the engine temperature ratio increased from 4 to 7, which is similar to the MIL to AB transition. Assuming a ~50% increase in the fully expanded jet velocity from MIL to afterburner, the value for κ is once again found to be between 0.64 and 0.7.

Between 140° to 160°, Fig. 3 shows little increase in OASPL from MIL to AB. According to Liu et al. [7], Leete et al. [21], and Vaughn et al. [8], this region is dominated by LSN. To explore which frequencies may be contributing to noise in this angular region, Fig. 4 shows frequency-dependent SPL directivity curves at each engine condition for different one-third octave bands, as measured at the 76 m arc. From MIL to AB between 140° and 160°, frequencies below 80 Hz increase in level, while frequencies above 80 Hz exhibit the far-aft saturation behavior seen in Fig. 3. A similar phenomenon has been observed in different afterburning military aircraft (e.g., James et al. [27]). The 315 Hz case in Fig. 4 also shows a distinct double lobe pattern at 50% thrust and 75% thrust, with one lobe at roughly 140° and the other further aft at about 155°. This double lobe phenomenon is also observed in the near-field by Olaveson et al. [22] and Mathews et al. [28]; both concurrent investigations also show that these lobes appear to come from distinct sources. At 75% thrust, the farthest aft lobe appears to reach its limit. Olaveson et al. show in their total field reconstructions that these lobes likely still exist but become washed out as the levels of the upstream lobe continue to grow.

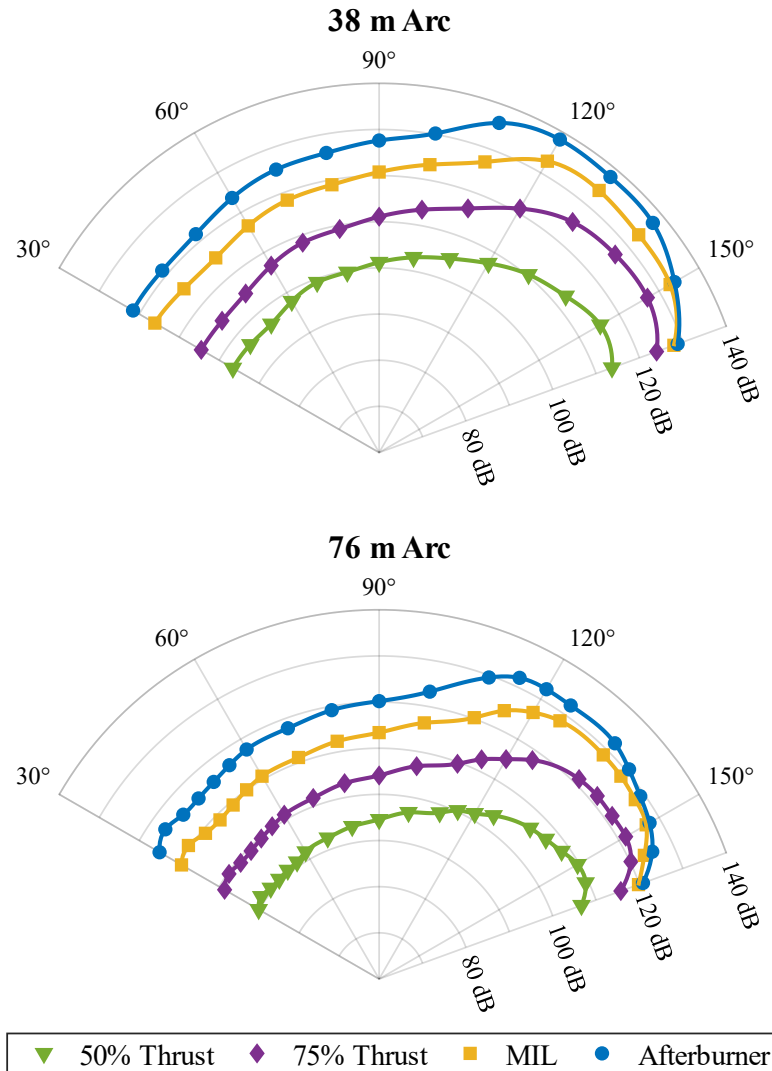


Fig 3: OASPL directivity curves at each engine power measured at the 38 m arc and 76 m arc.

Between 140° to 160° , Fig. 3 shows little increase in OASPL from MIL to AB. According to Liu et al. [7], Leete et al. [21], and Vaughn et al. [8], this region is dominated by LSN. To explore which frequencies may be contributing to noise in this angular region, Fig. 4 shows frequency-dependent SPL directivity curves at each engine condition for different one-third octave bands, as measured at the 76 m arc. From MIL to AB between 140° and 160° , frequencies below 80 Hz increase in level, while frequencies above 80 Hz exhibit the far-aft saturation behavior seen in Fig. 3. A similar phenomenon has been observed in different afterburning military aircraft (e.g., James et al. [27]). The 315 Hz case in Fig. 4 also shows a distinct double lobe pattern at 50% thrust and 75% thrust, with one lobe at roughly 140° and the other further aft at about 155° . This double lobe phenomenon is also observed in the near-field by Olaveson et al. [22] and Mathews et al. [28]; both concurrent investigations also show that these lobes appear to come from distinct sources. At 75% thrust, the farthest aft lobe appears to reach its limit. Olaveson et al. show in their total field reconstructions that these lobes likely still exist but become washed out as the levels of the upstream lobe continue to grow.

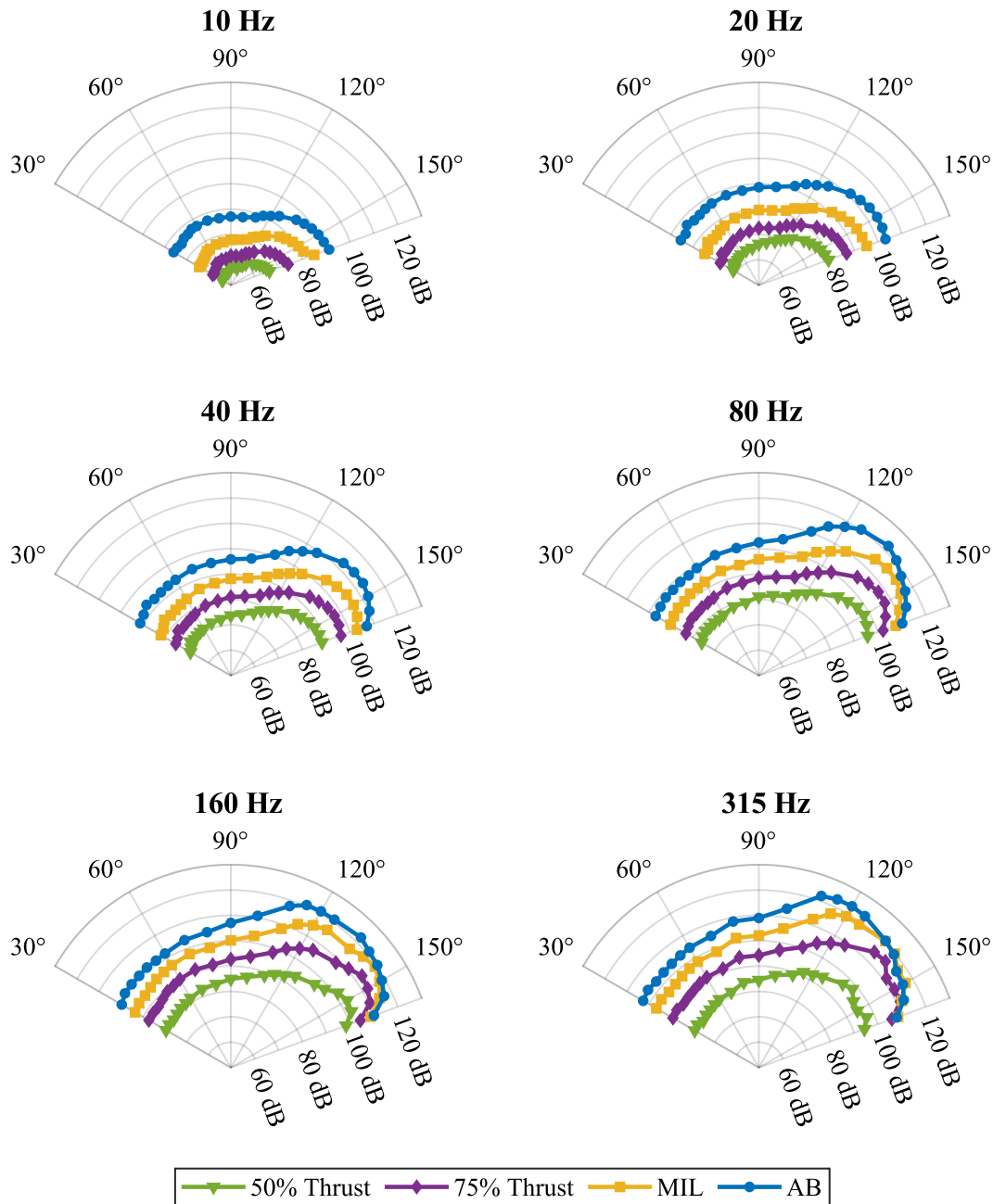


Fig 4: Frequency-dependent SPL plots from 10 Hz to 315 Hz, measured at AB at the 76 m arc.

Figure 5 shows spatio-spectral maps at each engine power from data taken at the 76 m arc. Visible are spatio-spectral lobes, which have been seen in several high-performance aircraft [9,22]. Though spatio-spectral lobes are most frequently seen in near-field analyses, Leete et al. [9] showed similar maps with data taken from a different aircraft, over a much more limited frequency range, but also along a 38 m arc. Further discussion of spatio-spectral lobes can be found in Olaveson et al. [22] and Mathews et al. [28].

At MIL and AB, Olaveson et al. [22] and Leete et al. [9] both show the presence of broadband shock-associated noise (BSN) upstream, between 500 Hz and 1 kHz. Figure 5 shows signs of BSN at MIL at AB in that frequency range, between 30° and 60°. Aft of 60°, regions of local minima are present between 600 Hz and 1 kHz, the same region where BSN would also be expected to be present with its peak also increasing in frequency. These nulls are

seen at all engine powers and are not explained by supersonic jet noise phenomena. Based on even simple-source round reflection models with the source at the MARP and a height of 1.5 m, the nulls are reasonably attributed to interference caused by ground reflections [29].

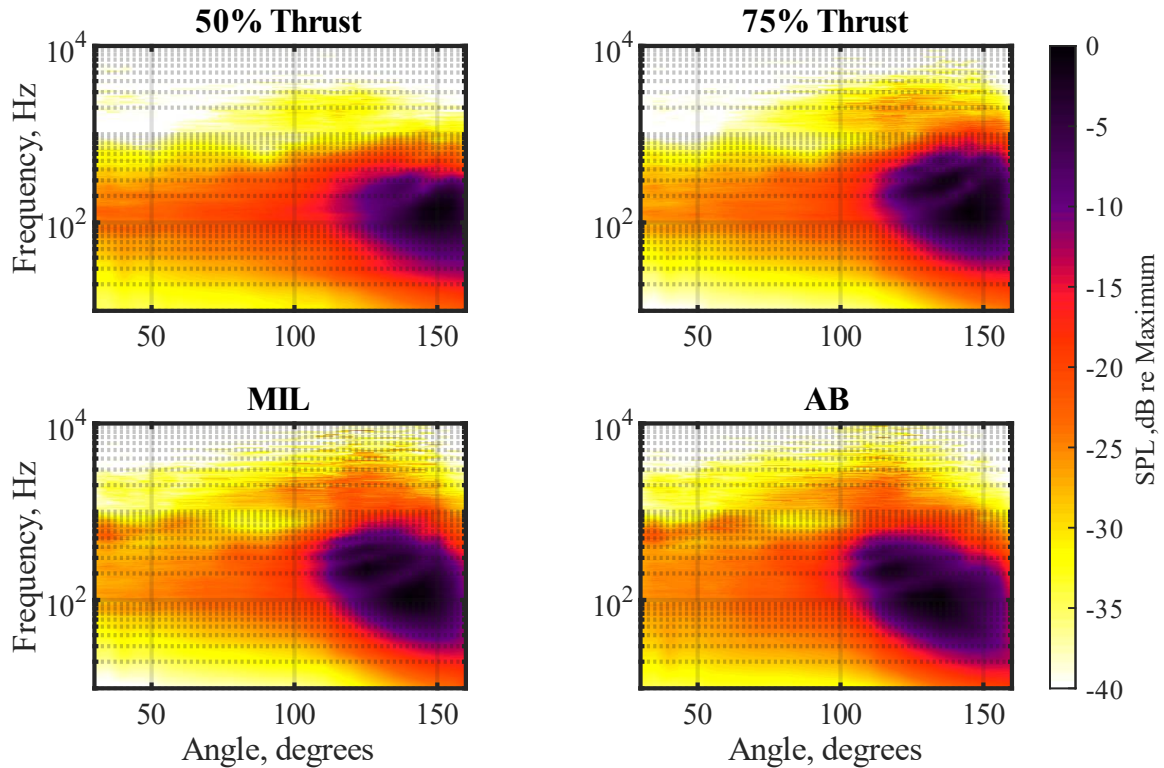


Fig 5: Spatospectral maps at each engine condition, measured from the 76 m arc.

B. Ground reflections

Interference from ground reflections introduces spectral changes that could impact the conclusions made in our study. To understand and potentially ameliorate these impacts, attempts were made to correct the spectra and minimize the effects of ground reflections on OASPL. As discussed in the introduction, the process used is based on the model developed by Gee et al. [12]. Building off the works of Daigle [10] and Johnson [11], Gee et al. developed an extended-source ground reflection model that accounts for a finite-impedance ground, as well as a turbulent atmosphere, both of which are factors that significantly affect the frequency-dependent effects of ground reflections on the measurements taken at the receiver. For sake of brevity, the coherent and incoherent-source models described in each of these sources will not be derived here.

From Gee et al.'s model, an initial attempt was made to correct for the effect of measurements being made above the ground. The jet is modeled as a discrete line source 2 m long, 1.5 m off the ground, with equally spaced sources. The coherence of the sources is presently unknown (but could be eventually modeled using the work of Morgan et al. [30] or Harker et al. [31]); therefore, the discrete line sources were modeled as both completely coherent and incoherent, providing a range of results. At HAFB, the ground at the test site beyond the runup pad consisted of packed dirt with little vegetation until beyond the 76 m arc. For this reason, the effective flow resistivity (related to the "hardness") of the ground was set to 700 cgs rayls for the 76 m arc and 1000 cgs rays for the 38 m arc. These values fall in the range of values described as roadside dirt in Embleton et al. [29]. Turbulence parameters – which were discussed by Gee et al. [12] to likely need to be larger near a rocket plume than in far-field – were adjusted empirically to produce overall smooth variation in spectra characteristics over a broad angular range. The model's empirical $\langle \mu^2 \rangle$ value, which accounts for mean-square turbulence fluctuation amplitudes, was found by subtracting the ground reflection spectra from the measured spectra and trying to smooth out the apparent nulls. These values were set to 1E-

4 for the 38 m arc and 1E-5 for the 76 m arc. Given how little is known about implementing these models in practice, a single ground reflection correction spectrum was found for all angles and engine conditions, to be subtracted from the measured spectrum. Figure 6 shows the effect of these ground reflection corrections on the power spectral density of three different microphones at AB, at 76 m. At low frequencies, there is a 6 dB reduction in level, corresponding to a coherent ground interaction, whereas at high frequencies, the reduction is closer to 3 dB (indicating that the coherence with a ground-induced image source is destroyed because of atmospheric turbulence). Additionally, the three angles show some of the impacts of the measurement and modeling choices around several hundred hertz. In the forward direction at 40°, the measurement geometry, unfortunately, caused an interference null to occur in the vicinity of the BSN spectral peak. This peak is partially reconstructed by the incoherent source model, but less so with the coherent source model – illustrating the importance of selecting microphone height and the sensitivity of source parameters. At 90°, the incoherent source model creates an FSN spectrum that is like the (free-field) fine-scale similarity spectrum discussed by Tam et al. [32], whereas the coherent source model does little to eliminate the interference null. Finally, at 150°, it is the coherent source model that does a better job of creating a smoother spectrum; the incoherent model creates too large of a spectral correction, resulting in a spectral bump. The lack of measured interference nulls at aft angles – seen in other full-scale aircraft and rocket measurements [33,34] – suggests a volumetric source that smears out interactions and means that there is no universal method for correcting for ground reflections, including simply placing microphones on the ground. The corrections presented here represent a preliminary work into the corrections of ground reflections, with parameters related to atmospheric turbulence being used to empirically smooth the nulls observed in the spectra of specific microphones. Further studies will be required to better understand and correct interference from ground reflections.

This same correction was applied to every microphone in both the 38 m and 76 m arcs. After making these corrections, new spatio-spectral maps were made from the 76 m arc by taking the mean of the coherent and incoherent sources models. These maps are shown in Fig. 7. Despite the rudimentary nature of the corrections, they fill in the gaps at about 1 kHz seen in the spatio-spectral maps in Fig. 5. As mentioned, one of the challenges associated with the ground reflection interference seen in the far-field is that the nulls appear at the same frequencies BSN is seen in the near field, as shown by Olaveson et al. [22] and Leete et al. [19]. Figure 7 shows that at MIL and AB, there appear to be signs of more smoothly varying BSN between 30° and 70° at about 600-800 kHz.

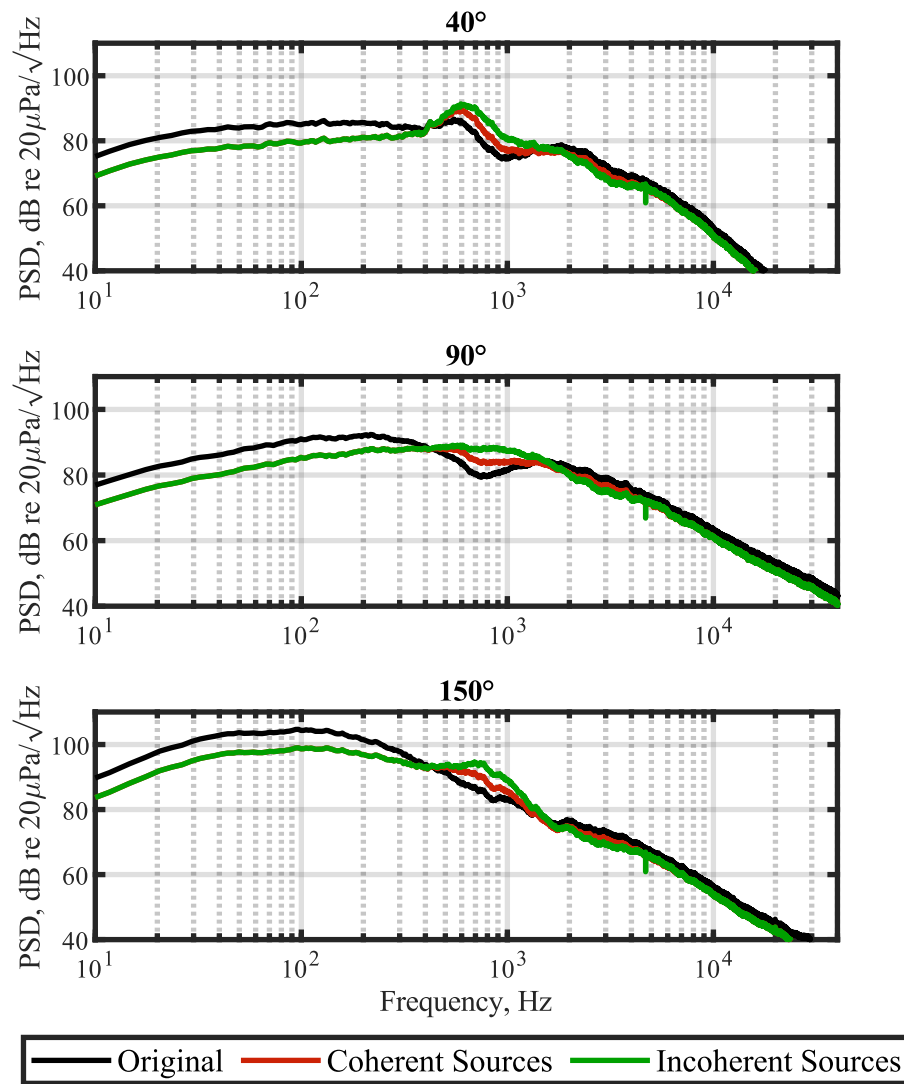


Fig. 6: Corrected power spectral densities at microphone angles of 40°, 90°, and 150° taken at AB at 76 m arc. Both incoherent and coherent sources are considered.

With a “free-field” version of the spatio-spectral map in Fig. 7, the spectra were summed to produce Fig. 8, which shows the changes in OASPL seen at each microphone along the 76 m arc. It is important to note for comparing to past measurements that the peak radiation angle and radiation lobe widths were unaffected by any of the ground reflection corrections. Note that the maximum OASPL did decrease by as much as 5 dB in the 50% thrust case at the far-aft angles. In the forward direction, both source models generally decreased the OASPL at 50% thrust and 75% thrust but added to the OASPL at MIL and AB. This can be explained by the BSN which appears to have been nullified by ground reflections. Overall, though, the most important conclusion from Fig. 8 is that accounting for ground reflections is not a simple 3 dB subtraction (removal of an incoherent image source). Nor is it between 3-6 dB at all angles, as has been suggested for a partially coherent source. The effect at dominant radiation angles is as little as 1 dB and as large as 5 dB per the Gee et al. [12] methodology with simple coherent/incoherent line-source models. But to determine the “overall” effect on radiation, a sound power integration can be performed.

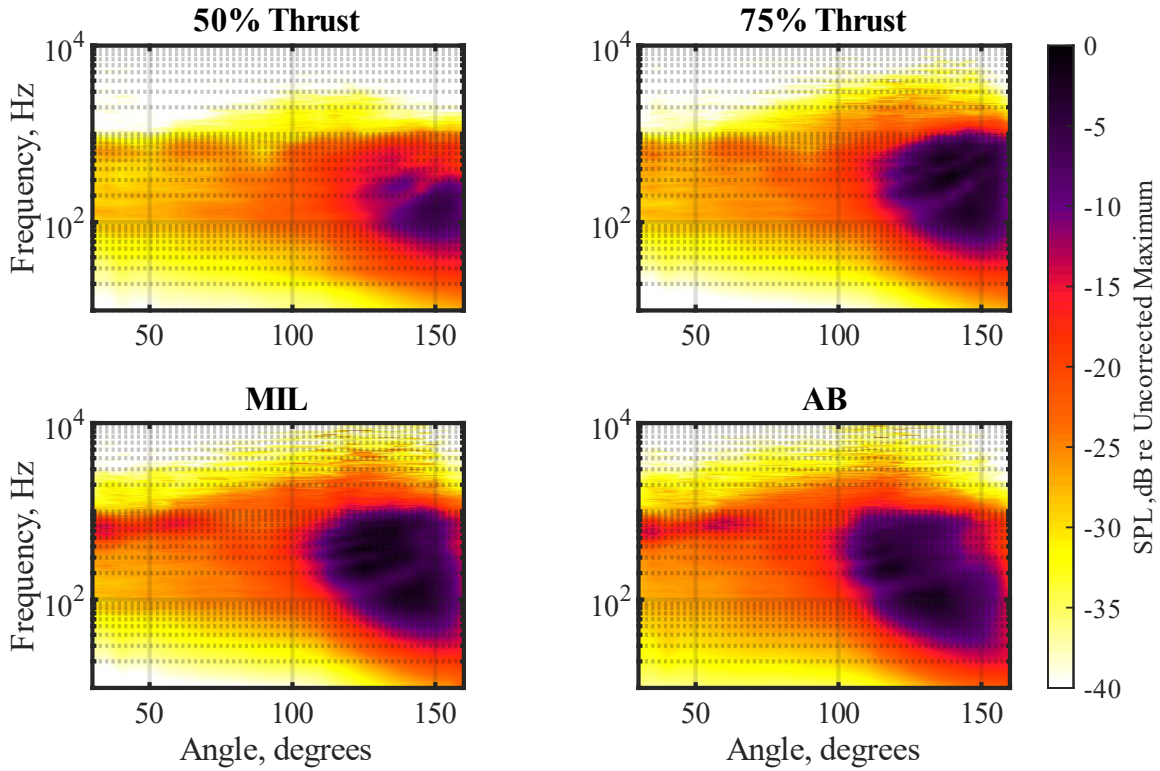


Fig 7: Spatio-spectral maps at each engine power after correcting for ground reflections.

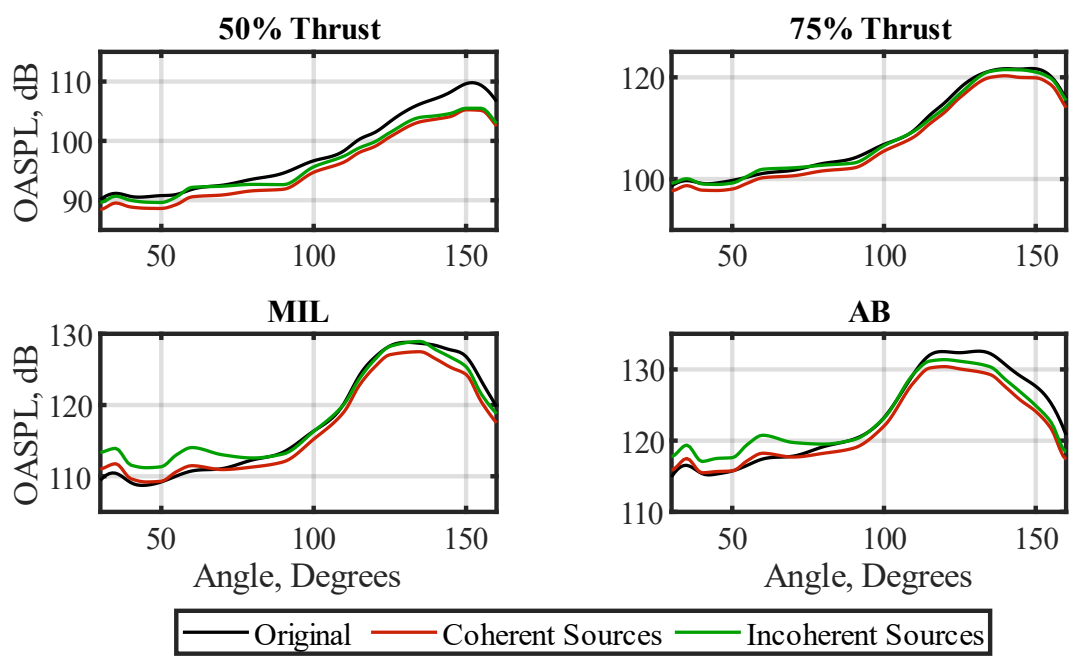


Fig 8: OASPL directivity curves from original measurement compared against the ground reflection corrected values.

C. Sound power and acoustic radiation efficiency

Sound power is a useful metric in understanding the overall radiation output from a source. Sound power can be measured from a source by integrating the intensity across all angles:

$$\bar{\Pi} = \int_S \bar{I} \cdot n_{out} dS, \quad (3)$$

where \bar{I} represents the time-averaged acoustic intensity at some surface, S , with n_{out} representing the outward-facing normal vector of that surface. The sound power from supersonic jets has been described somewhat frequently in rocket noise literature [13,15,35,36], whereas the OASPL in the peak radiation direction often serves as a surrogate for OAPWL in the jet noise literature. The study of sound power in launch vehicles has been useful because it provides a connection between what is mechanically happening in the engine and what is radiated. One of these connections is the acoustic radiation efficiency (η_{ac}), which is simply the ratio of acoustic power to the mechanical power output from the source,

$$\eta_{ac} = \frac{\Pi_{ac}}{\Pi_m}. \quad (4)$$

Though common in rocket literature, discussion of sound power and η_{ac} has been fairly limited in the field of military aircraft noise. Sound power from aircraft engines was shown and discussed by Franken [16] in 1958, but such discussion has been largely absent in contemporary literature. Here, we show the process used for calculating sound power from the far-field measurements taken from the T-7A, as well as the preliminary results achieved when looking at η_{ac} . Observing changes in η_{ac} may be an appropriate figure of merit when describing jet noise reduction methods.

The process used to calculate sound power is based on Leishman et al. [37], as implemented for various scales of jets (laboratory, aircraft, rocket, and volcano) by Matoza et al. [17]. The integral in Eq. 3 can be approximated using the summation:

$$\bar{\Pi} = \sum_{l=1}^L \bar{\Pi}_l = \sum_{l=1}^L \bar{I}(\theta_l) \Delta S(\theta_l) \quad (5)$$

Matoza et al. describe the value $\Delta S(\theta_l)$ as a weighting factor that covers the effective sampling area of each microphone in the array. For a polar array at a single azimuthal angle, azimuthal symmetry must be assumed. For this axisymmetric, free-field case, Leishman et al. [37] defined $\Delta S(\theta_l)$ as:

$$\Delta S(\theta_l) = \begin{cases} 4\pi r^2 \sin^2\left(\frac{\Delta\theta_l}{4}\right) & \text{for } l = 1, L \\ 4\pi r^2 \sin\left(\frac{\theta_l}{4}\right) & \text{for } 2 \leq l \leq L - 1 \end{cases} \quad (6)$$

By assuming far-field behavior, the time-averaged squared pressure, $\overline{p^2}$, and intensity can be simply related using:

$$I = \frac{\overline{p^2}}{\rho c} \quad (7)$$

The use of Eq. (6) with Eq. (5) provides the time-averaged acoustic power in watts, which can be converted to OAPWL as

$$\text{OAPWL} = 10 \log_{10} \left(\frac{\bar{\Pi}}{\Pi_{ref}} \right), \quad (8)$$

where $\Pi_{ref} = 1$ pW. Because the calculation requires intensity values from 0° to 180° , but measurements in the far-field only spanned angles from 30° to 160° , values at the missing angles had to be estimated. OASPL values at 0° were set to the minimum OASPL value of the given engine power. For values at 180° , the rate at which OASPL changed from 155° to 160° was calculated, then assumed to be constant from 155° to 180° . OASPL values were interpolated at 1° increments from 0° to 180° from these and the measured values, using MATLAB's `pchip` function.

The F404 OAPWL values were calculated using the ground reflection corrected OASPL values from Fig. 8, as well as for ground reflections calculated from the 38 m data. The range of OAWPL values calculated at both 38 m and 76 m arcs are reported in Table 2. The range of levels in Table 2 includes the raw data, and the data corrected for ground reflections from coherent and incoherent sources. The jet data extrapolated from Ennix [20] and Seiner [3] were used to develop an estimate for the mechanical power output of the F-404 engine exhaust using Eq. (9), where F represents the thrust from the engine [38]:

$$\Pi_m = \frac{1}{2} U_j F. \quad (9)$$

From the values of Π_m calculated, Eq. (4) was used to provide a range of acoustic efficiencies at each engine power, shown in Table 2.

Table 2: OAWPL and acoustic efficiency values measured from the T-7A at both 38 m and 76 m arcs.

Engine Power	OAPWL	η_{ac} , %
50% Thrust	145.6 – 149.8	0.01 – 0.02
75% Thrust	159.2 – 162.8	0.08 – 0.19
MIL	167.6 – 170.7	0.34 – 0.70
AB	172.2 – 175.4	0.41 – 0.85

Figure 9 shows the F404 OAPWL plotted as a function of mechanical power for all four engine conditions. Both the 38 m and 76 m data ground-reflection results are included in the ranges, for the coherent and incoherent line source corrections, as well as the average for the four conditions. The calculated OAPWL from both the 38 and 76 m measurements is also shown. The error bars represent the range in Seiner vs Ennix values and the vertical range, the ground corrected OAPWLs from both distances. The measurement-based values are extremely similar for the two polar arcs, and the ground-reflection correction impact becomes less as engine power increases. At 50% thrust, the model-average correction is about 4 dB, whereas for MIL and AB the reduction in OAPWL is about 2 dB. The overall increase in OAPWL with engine condition is smoothly varying, but nonlinear on this (effective) log-log scale.

This trend of OAPWL vs Π_m can be examined in context of classical jet noise theory. Lighthill [4] indicated that sound power was proportional to the jet velocity of the jet to the eighth power (U_e^8). Because Π_m can be shown to increase as U_e^3 (see Lubert et al. [14]), this translates to a 50 dB/decade slope in Fig. 9, shown as the black dashed line. The transition from 50% to 75% thrust is well approximated by this slope, even accounting for the ranges of Π_m and OAPWL shown. This helps to confirm the prior evidence that 50% thrust jet conditions are within the subsonic regime and indicates that the 50% to 75% thrust transitions fall within the subsonic regime. This also suggests that the transition from 75% to MIL transition falls within the transonic or weakly supersonic regime. The transition from MIL to AB (both supersonic because of MWR and BSN evidence) shows classical supersonic jet noise behavior. Early measurements by Chobotov and Powell [18] and theory by Ffowcs Williams [5] indicated that sound power for supersonic jets transitions from the U_e^8 law to being proportional to the jet velocity to the third power, U_e^3 . (See Lubert et al. [14] for a modern, dimensionally correct version of the classical Chobotov and Powell figure.) Given the U_e^3 of Π_m , this is a linear relationship between Π_m and Π_{ac} , which is translated into the red dashed 10 dB/decade line in Fig. 9. Even considering the range of values shown, the slope from the MIL and AB OAPWLs is approximately 10 dB/decade, indicating agreement with classical theory. To the authors' knowledge, and even within the uncertainty of the F404-103 operational parameters, even approximate agreement with classical theory has not been demonstrated for modern high-performance jet engines.

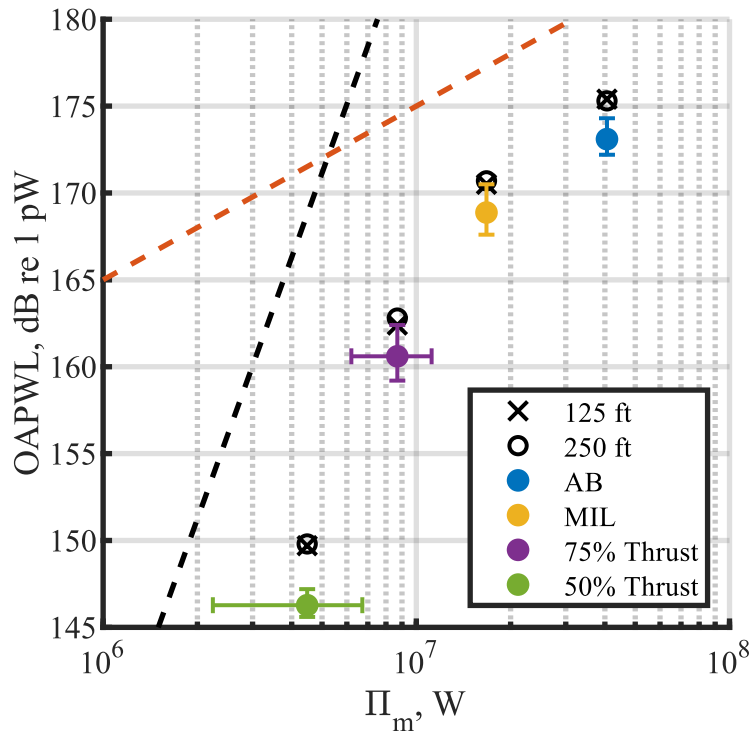


Figure 9: OAPWL measured from 38 m and 76 m arcs plotted as a function of the estimated Π_m from the F404 engine. Data points in black represent raw data points, not accounting for ground reflections. The dashed black line represents a 50 dB/decade increase, and the dashed red line represents a 10 dB/decade increase.

Whereas η_{ac} increases with U_e for subsonic jets, for supersonic jets, the linear dependence of Π_{ac} on Π_m suggests a constant η_{ac} . Franken [16] described η_{ac} trends for jet engines in 1958. Franken reported afterburning aircraft have an η_{ac} between 0.75% and 1% with turbojets being approximately 0.5% efficient. In 1963, Ffowcs Williams [5] suggested an upper bound of 0.6%. In 1971, Eldred [13] reported η_{ac} for several rockets, with considerable data scatter but with most of the rockets surveyed being between 0.2 and 0.5% efficient. Figure 10 shows the T-7A values at MIL and AB compared with some of the data reported by Eldred. The ground-reflection-corrected T-7A data points fit in well with data from NASA SP-8072, with average values sitting almost exactly on the 0.5% value assumed by Eldred for rockets. This indicates that at its highest engine powers, the T-7A acoustically behaves similarly to rockets within similar Π_m . It is also important to note that lower engine powers have lesser radiation efficiencies. The large increase in efficiency between 75% thrust and MIL suggests a critical change in jet conditions. That is not to say that all supersonic jets follow this trend. Leete et al. [21] calculated η_{ac} for the AB-like LES results of Liu et al. [7] and found an efficiency of $\sim 1.5\%$, which is far enough from $\eta_{ac} \approx 0.5\%$ to merit investigation. Likewise, Mathews et al. [15] finding $\eta_{ac} \approx 0.31\%$ for the Falcon 9 – averaged over three launches and several locations – even without accounting for ground reflections suggests that there is more to learn.

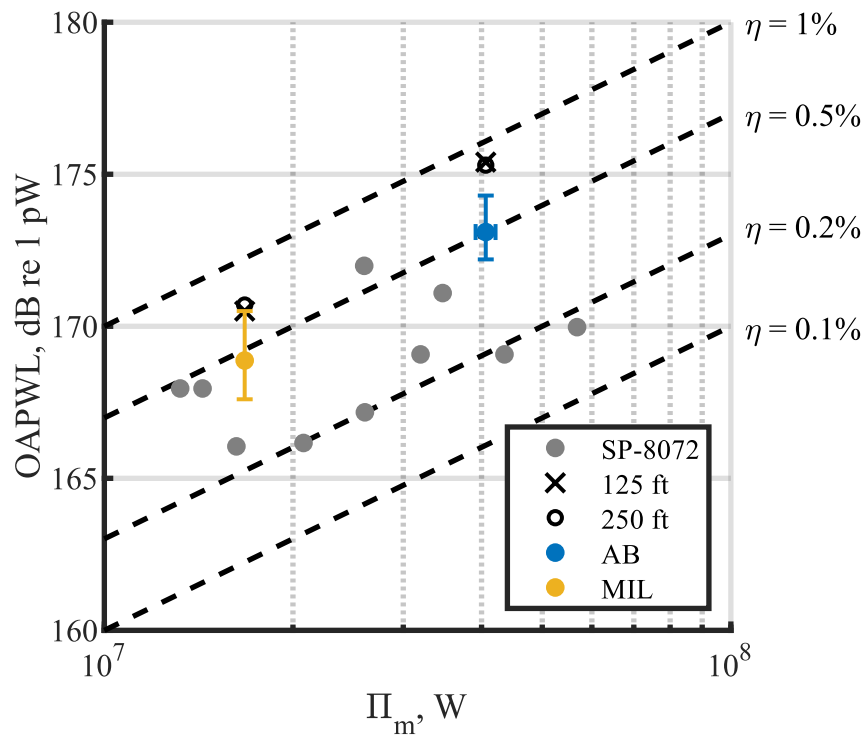


Figure 10: T-7A values at MIL and AB plotted alongside rocket values reported by Eldred in NASA SP-8072 [13].

D. Directivity Index

With directivity and sound power, directivity indices can be calculated for the T-7A as a function of engine condition. A directivity index (DI) is defined as the difference in SPL, as a function of angle, between what was measured and what would be measured from a monopole with an equivalent sound power. Using the OAPWL calculated for the T-7A, working backward through the above process, but assuming constant intensity across all angles, yields the sound intensity level of a monopole. Subtracting the equivalent monopole SPL for a source from the measured SPL as a function of angle yields the DI, as discussed in Manhart et al. [39]. The DI of the T-7A is shown in Fig. 11. Like Fig. 3, Fig. 11 shows that the peak radiation inlet angle decreases as engine power increases. It also indicates that the peak jet radiation angle broadens as jet temperature increases, illustrated by the peak value decreasing but the angular span over which the index is positive increasing. There is a significant difference noted between 50% thrust and 75% thrust, where the angles farthest upstream decrease by as much as 5 dB, indicating a significant acoustic change between the two engine conditions. This large change in acoustic levels, also seen in F-35A analyses for the same change in relative thrust range, is likely an important regime of supersonic jet conditions to explore in the pursuit of noise reduction strategies.

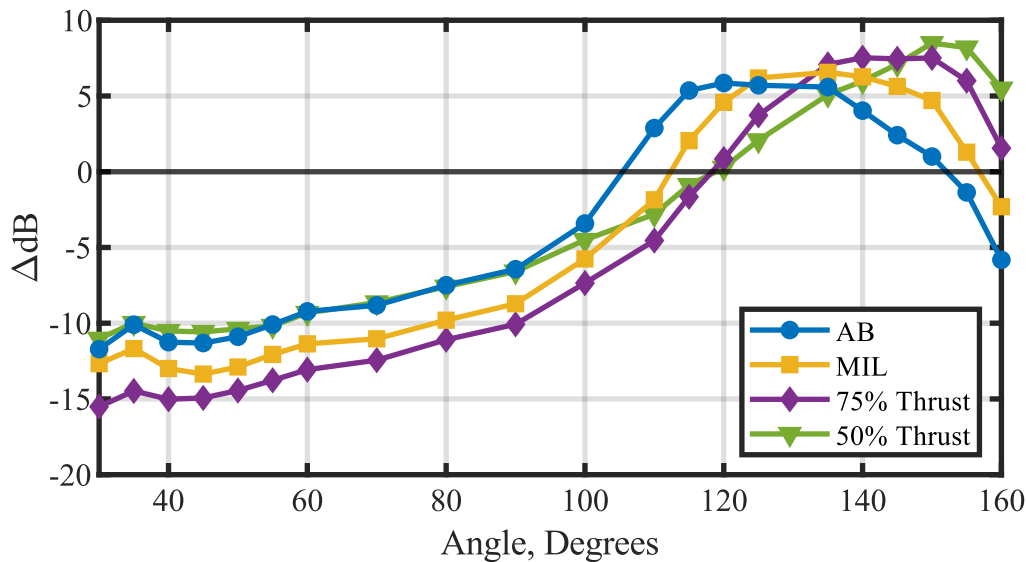


Figure 11: Directivity index at each engine power, measured from 76 m arc.

The peak DI is a topic of interest in simple models for determining maximum expected sound levels from a jet with a given OAPWL. The peak DI for rocket noise is shown by McInerny [36] and Cole et al. [35] to range from 5 to 8 dB. In examining the data of Mathews et al. [15], the peak DI of the Falcon 9 vehicle is found to be ~8 dB. For the T-7A, the peak DI is seen to decrease with increasing engine power, settling at approximately 6 dB at full afterburner. This is less than the 8 dB peak directivity index shown by Franken [16] for a turbojet engine. However, note that a peak directivity angle of ~140° in Franken's example would be like the 75% thrust case shown here, which has a peak DI slightly less than 8 dB. At present, to our best understanding, the peak directivity index for tactical jet engines is 6-8 dB, regardless of condition.

V. Conclusion

This paper explores connecting far-field acoustic data with source characteristics from measurements taken from a GE F404-103 engine installed in a Boeing/SAAB T-7A "Red Hawk." Using data from 38m and 76 m arcs, directivity curves were evaluated at engine powers from 50% thrust to AB. The peak radiation angle is shown to decrease with increasing engine power. It appeared that MWR played an important role in the far-field directivity at MIL and AB, indicating a supersonic jet. The directivity curves indicate a saturation in the levels farthest aft from MIL to AB, a phenomenon also seen in other far-field acoustic studies of high-performance afterburning jet engines [27]. Frequency-dependent directivity curves illustrate this further, showing frequencies above 80 Hz remain static from MIL to AB. Spatiospectral maps of the 76 m far-field data show the presence of spatio-spectral lobes, like those seen in the near-field, as reported by both Olaveson et al. [22] and Mathews et al. [28]. The same maps show the likely presence of BSN, though nulls from ground reflections appear in the frequency range where additional BSN would be expected.

Ground reflection interference significantly affected the data collection in the far-field. To account for these effects, the ground reflection correction model developed by Gee et al. [12] was used to correct spectra at each microphone in the 76 m arc. The spatio-spectral maps of these corrected spectra show increased BSN in the regions where nulls had previously been. These results, though preliminary, more realistically remove the effects of ground reflections on overall level, sound power, and acoustic radiation efficiency (η_{ac}).

Though largely absent in contemporary military aircraft noise studies, sound power and η_{ac} are useful metrics for connecting far-field acoustical observations and jet characteristics. After correcting for ground reflections, OAPWL and η_{ac} were evaluated at each engine power. The relationship between OAPWL and mechanical power was compared with classical jet noise theory. It was shown that from 50% thrust to 75% thrust, sound power was proportional to U_e^3 , as predicted by Lighthill [4], and was proportional to U_e^3 from MIL to AB, exhibiting the characteristics of a supersonic jet as described by Chobotov and Powell [18] and Ffowcs Williams [5]. At MIL and AB, η_{ac} was found to be roughly

0.5%, which is like the values for rockets reported by Eldred in 1971 [13]. Finally, the peak directivity index decreased with increasing engine power, with AB showing a peak directivity index of 6 dB.

Acknowledgments

The authors gratefully acknowledge the funding provided by the Office of Naval Research under grant number N00014-21-1-2069 with project monitor Dr. Steven Martens, Code 351 Jet Noise Reduction. Measurements were funded through the Advanced Pilot Training System Program Office and the Air Force Research Laboratory. Distribution A. Approved for public release; distribution unlimited; Cleared 25 May 2022; 43-9694-22.

References

- [1] Casalino, D., Diozzi, F., Sannino, R., and Paonessa, A. "Aircraft Noise Reduction Technologies: A Bibliographic Review." *Aerospace Science and Technology*, Vol. 12, No. 1, 2008, pp. 1–17. <https://doi.org/10.1016/j.ast.2007.10.004>.
- [2] Greska, B. J., Krothapalli, A., Seiner, J. M., Jansen, B., and Ukeiley, L. "The effects of microjet injection on an F404 jet engine," AIAA Paper 2005-3047.
- [3] Seiner, J. M., Ukeiley, L. S., and Jansen, B. J. "Aero-Performance Efficient Noise Reduction for the F404-400 Engine." AIAA Paper 2005-3048
- [4] Lighthill, M. J. "On Sound Generated Aerodynamically: I. General Theory." *Proceedings of the Royal Society*, 1952, pp. 564–587.
- [5] Ffowcs Williams, J. E. "The Noise from Turbulence Convected at High Speed." *Philosophical Transactions of the Royal Society of London. Series A, Mathematical and Physical Sciences*, Vol. 255, No. 1061, 1963, pp. 469–503. <https://doi.org/10.1098/rsta.1963.0010>.
- [6] Tam, C. K. W., and Hu, F. Q. "On the Three Families of Instability Waves of High-Speed Jets." *Journal of Fluid Mechanics*, Vol. 201, 1989, pp. 447–483. <https://doi.org/10.1017/S002211208900100X>.
- [7] Liu, J., Corrigan, A., Kailasanath, K., and Taylor, B. "Impact of the Specific Heat Ratio on the Noise Generation in a High-Temperature Supersonic Jet." *54th AIAA Aerospace Sciences Meeting*, Vol. 0, No. January, 2016, pp. 1–26. <https://doi.org/10.2514/6.2016-2125>.
- [8] Vaughn, A. B., Gee, K. L., Swift, S. H., Leete, K. M., Wall, A. T., Downing, J. M., and James, M. M. "Source Localization of Crackle-Related Events in Military Aircraft Jet Noise." *AIAA Journal*, Vol. 59, No. 6, 2021, pp. 2251–2261. <https://doi.org/10.2514/1.j059823>.
- [9] Leete, K. M., Wall, A. T., Gee, K. L., Neilsen, T. B., James, M. M., and Downing, J. M. "Acoustical Holography-Based Analysis of Spatiospectral Lobes in High-Performance Aircraft Jet Noise." *AIAA Journal*, Vol. 59, No. 10, 2021, pp. 4166–4178. <https://doi.org/10.2514/1.j059400>.
- [10] Daigle, G. A. "Effects of Atmospheric Turbulence on the Interference of Sound Waves above a Finite Impedance Boundary." *Journal of the Acoustical Society of America*, Vol. 65, No. 1, 1979, pp. 45–49. <https://doi.org/10.1121/1.382265>.
- [11] Johnson, M. A., Raspet, R., and Bobak, M. T. "A Turbulence Model for Sound Propagation from an Elevated Source above Level Ground." *Journal of the Acoustical Society of America*, Vol. 81, No. 3, 1987, pp. 638–646. <https://doi.org/10.1121/1.394831>.
- [12] Gee, K. L., Neilsen, T. B., and James, M. M. "Including Source Correlation and Atmospheric Turbulence in a Ground Reflection Model for Rocket Noise." *Proceedings of Meetings on Acoustics*, Vol. 22, No. 1, 2015. <https://doi.org/10.1121/2.0000002>.
- [13] Eldred, K. M. "Acoustic Loads Generated by the Propulsion System." NASA SP-8072. 1971.

- [14] Lubert, C. P., Gee, K. L., and Tsutsumi, S. "Supersonic Jet Noise from Launch Vehicles: 50 Years since NASA SP-8072." *The Journal of the Acoustical Society of America*, Vol. 151, No. 2, 2022, pp. 752–791. <https://doi.org/10.1121/10.0009160>.
- [15] Mathews, L. T., Gee, K. L., and Hart, G. W. "Characterization of Falcon 9 Launch Vehicle Noise from Far-Field Measurements." *The Journal of the Acoustical Society of America*, Vol. 150, No. 1, 2021, pp. 620–633. <https://doi.org/10.1121/10.0005658>.
- [16] Franken, P. A. "Review of Information on Jet Noise." *Noise Control*, Vol. 4, No. 3, 1958, pp. 8–16. <https://doi.org/10.1121/1.2369320>.
- [17] Matoza, R. S., Fee, D., Neilsen, T. B., Gee, K. L., and Ogden, D. E. "Aeroacoustics of Volcanic Jets: Acoustic Power Estimation and Jet Velocity Dependence." *Journal of Geophysical Research: Solid Earth*, Vol. 118, No. 12, 2013, pp. 6269–6284. <https://doi.org/10.1002/2013JB010303>.
- [18] Chobotov, V., and Powell, A. "On the Prediction of Acoustic Environments from Rockets." Rama-Wooldridge Corporation Report E.M.-7-7. 1957.
- [19] Leete, K. M., Vaughn, A. B., Bassett, M. S., Rasband, R. D., Novakovich, D. J., Gee, K. L., Campbell, S. C., Mobley, F. S., and Wall, A. T. "Jet Noise Measurements of an Installed Ge F404 Engine." AIAA Paper 2021-1638.
- [20] Ennix, K., Burcham, Jr., F., and Webb, L. "Flight-Determined Engine Exhaust Characteristics of an F404 Engine in an F-18 Airplane." NASA Technical Memorandum 4538. 1993. <https://doi.org/10.2514/6.1993-2543>.
- [21] Leete, K. M., Gee, K. L., Liu, J., and Wall, A. T. "Near-Field Acoustical Holography and Acoustic Power Analysis of a Simulated, Highly Heated Supersonic Jet." Vol. 1989, 2022. <https://doi.org/10.1121/10.0009827>.
- [22] Olaveson, T., Ward, J. A., Johnson, J. P., Gee, K. L., and Wall, A. T. "Analysis of Spatospectral Lobes in Installed F404 Engine Noise Radiation." *28th AIAA/CEAS Aeroacoustics Conference*, 2022 (not yet published).
- [23] Seiner, J. M., and Ponton, M. K. "The Effects of Temperature on Supersonic Jet Noise Emission." AIAA Paper 92-2046.
- [24] Tam, C. K. W., and Parrish, S. A. "Noise of High-Performance Aircraft at Afterburner." *Journal of Sound and Vibration*, Vol. 352, 2015, pp. 103–128. <https://doi.org/10.1016/j.jsv.2015.04.010>.
- [25] Murray, N. E., and Lyons, G. W. "On the Convection Velocity of Source Events Related to Supersonic Jet Crackle." *Journal of Fluid Mechanics*, Vol. 793, 2016, pp. 477–503. <https://doi.org/10.1017/jfm.2016.127>.
- [26] Chen, S., Gojon, R., and Mihaescu, M. "Flow and Aeroacoustic Attributes of Highly-Heated Transitional Rectangular Supersonic Jets." *Aerospace Science and Technology*, Vol. 114, 2021, p. 106747. <https://doi.org/10.1016/j.ast.2021.106747>.
- [27] James, M. M., Salton, A. R., Downing, J. M., Gee, K. L., Neilsen, T. B., Reichman, B. O., Mckinley, R. L., Wall, A. T., Gallagher, H. L. "Acoustic Emissions from F-35 Aircraft during Ground." AIAA Paper 2015-2375
- [28] Mathews, L. T., Gee, K. L., and Leete, K. M. "Acoustic Source Characterization of an Installed GE F404 Engine Using Near-Field Acoustical Holography." *28th AIAA/CEAS Aeroacoustics Conference*, 2022 (not yet published).

- [29] Embleton, T. F. W., Piercy, J. E., and Daigle, G. A. "Effective Flow Resistivity of Ground Surfaces Determined by Acoustical Measurements." *The Journal of the Acoustical Society of America*, Vol. 74, No. 4, 1983, pp. 1239–1244. <https://doi.org/10.1121/1.390029>.
- [30] Morgan, J., Neilsen, T. B., Gee, K. L., Wall, A. T., and James, M. M. "Simple-Source Model of Military Jet Aircraft Noise." *41st International Congress and Exposition on Noise Control Engineering 2012, INTER-NOISE 2012*, Vol. 10, No. February, 2012, pp. 8410–8421.
- [31] Harker, B. M., Gee, K. L., Neilsen, T. B., Wall, A. T., and James, M. M. "Beamforming-Based Wavepacket Model for Noise Environment Predictions of Tactical Aircraft." AIAA Paper 2017-4048.
- [32] Tam, C. K. W., Viswanathan, K., Ahuja, K. K., and Panda, J. "The Sources of Jet Noise: Experimental Evidence." *Journal of Fluid Mechanics*, Vol. 615, 2008, pp. 253–292. <https://doi.org/10.1017/S0022112008003704>
- [33] Gee, K. L., Giraud, J. H., Blotter, J. D., and Sommerfeldt, S. D. "Energy-Based Acoustical Measurements of Rocket Noise." AIAA Paper 2009-3165. <https://doi.org/10.2514/6.2009-3165>.
- [34] Reichman, B. O., Gee, K. L., Neilsen, T. B., Hales Swift, S., Wall, A. T., Gallagher, H. L., Micah Downing, J., and James, M. M. "Acoustic Shock Formation in Noise Propagation during Ground Run-up Operations of Military Aircraft." AIAA Paper 2017-404. <https://doi.org/10.2514/6.2017-4043>.
- [35] Cole, J. N., von Gierke, H. E., Kyrasis, D. T., Eldred, K. M., and Humphrey, A. J. Noise Radiation from Fourteen Types of Rockets in the 1,000 to 130,000 Pounds Thrust Range. *Wright Air Development Center, TR. 57–354*.
- [36] Mcinerny, S. A. (University of A. Launch Vehicle Acoustics Part 1: Overall Levels and Spectral Characteristics. *Journal of Aircraft*. 3. Volume 33, 511–517. <https://arc.aiaa.org/doi/10.2514/3.46974>.
- [37] Leishman, T. W., Rollins, S., and Smith, H. M. "An Experimental Evaluation of Regular Polyhedron Loudspeakers as Omnidirectional Sources of Sound." *The Journal of the Acoustical Society of America*, Vol. 120, No. 3, 2006, pp. 1411–1422. <https://doi.org/10.1121/1.2221552>.
- [38] Varnier, J. "Experimental Study and Simulation of Rocket Engine Freejet Noise." *AIAA Journal*, Vol. 39, No. 10, 2001, pp. 1851–1859. <https://doi.org/10.1207/s15327752jpa8502>.
- [39] Manhart, J. K., Ailman, C. M., Lane, S. R., and Marsh, A. H. "An Acoustical Study of the KIWI B Nuclear Rocket." NASA CR-370. 1966.